Volume 146
Number 7
7 April 2021
Pages 2085-2402

Analyst

rsc.li/analyst

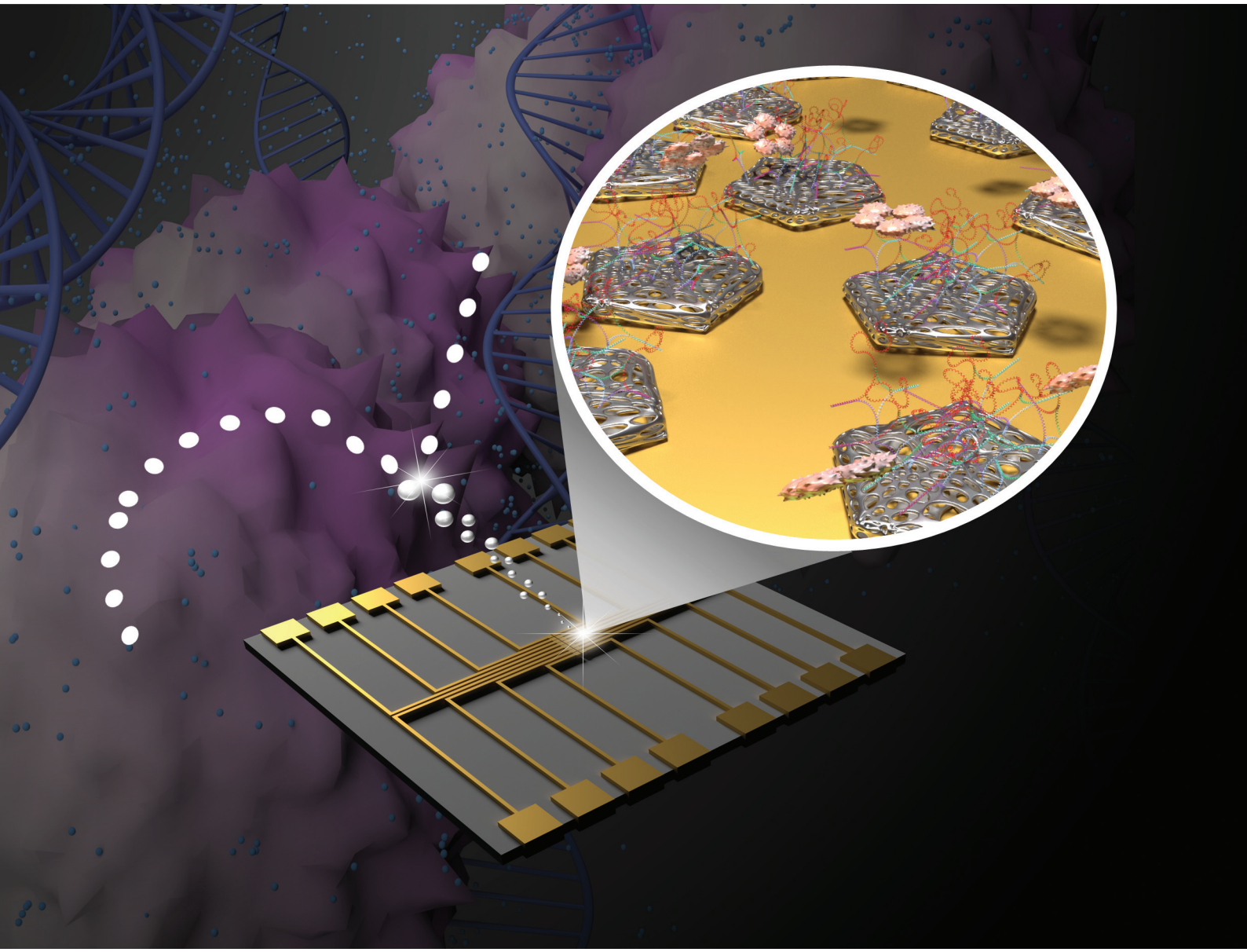

ISSN 0003-2654

ROYAL SOCIETY OF CHEMISTRY

PAPER

Taek Lee *et al.*

Fabrication of an electrochemical biosensor composed of multi-functional Ag ion intercalated DNA four-way junctions/rhodium nanoplate heterolayer on a micro-gap for C-reactive protein detection in human serum

Analyst

ROYAL SOCIETY OF CHEMISTRY

PAPER

View Article Online
View Journal | View Issue

Cite this: *Analyst*, 2021, **146**, 2131

Fabrication of an electrochemical biosensor composed of multi-functional Ag ion intercalated DNA four-way junctions/rhodium nanoplate heterolayer on a micro-gap for C-reactive protein detection in human serum†

Jinmyeong Kim,[a] Jeong-Ah Park,[a] Gyeonghye Yim,[b] Hongje Jang,[b] Tae-Hyung Kim,[c] Hiesang Sohn[a] and Taek Lee *[a]

As inflammation plays a role in the pathogenesis of acute coronary syndromes, C-reactive protein (CRP) can be used as a biomarker. To detect CRP precisely, the authors prepared a CRP electrochemical biosensor consisting of an eight Ag ion-intercalated multifunctional DNA four-way junction (MF-DNA-4WJ) and a porous rhodium nanoparticle (pRhNP) heterolayer on a micro-gap electrode. To increase conductivity, we used eight Ag^+ ion-inserted DNA four-way junctions through a C–C mismatch. Each DNA 4WJ was designed to have the CRP aptamer sequence, an anchoring region (thiol group), and two of four C–C mismatch regions at the end of the fragments. After an annealing step, the MF-DNA-4WJ assembly configuration and selective binding of CRP were confirmed through native TBM–PAGE (Tris-borate-magnesium chloride–polyacrylamide gel electrophoresis). The Au micro-gap electrode was fabricated to load 5 μl of the sample, and this was performed during eight experiments on one chip to establish the accuracy of the data. Then, pRhNPs were immobilized on a Au micro-gap electrode using cysteamine. To confirm the electrochemical properties, cyclic voltammetry (CV) and electrochemical impedance spectroscopy (EIS) were conducted. The durability of pRhNPs was confirmed through CV. To test the sensing performance of the prepared CRP biosensor, the limit of detection (LOD) and selectivity tests were conducted using EIS. The results indicated that charge transfer resistance (R_{ct}) can be used efficiently to probe these interactions within the variable CRP concentration range, from 1 pM to 100 nM (0.23 ng L^{-1}–23 μg L^{-1}). The LOD of this sensor was 0.349 pM (0.08 ng L^{-1}) (at S/N = 3). As a result of diluting the CRP to the same concentration range in a 20% human serum sample, the LOD was 3.55 fM (0.814 pg L^{-1}) (at S/N = 3).

Received 28th October 2020,
Accepted 23rd December 2020

DOI: 10.1039/d0an02135k

rsc.li/analyst

Introduction

Conventionally, the development of medicine and pharmacy has extended lives and improved the welfare of humans across the world. In addition, the rise of biotechnology offers the opportunity to further develop various concepts of drugs,[1,2] biomarkers,[3,4] and diagnostic tools.[5,6] Moreover, the convergence of medicine, pharmacy, and biotechnology has led to innovative drugs and clinical diagnostic methods that increase the survival rate of acute diseases, including acute myocardial infarction (AMI),[7,8] hypertension,[9,10] and immune system diseases.[11,12] Recent advances in information and communication technology (ICT) with nanobiotechnology (NBT) have resulted in the rapid development of healthcare services and *in vitro* diagnostic devices (IVDDs).[13–15] These IVDDs can be designed to connect with a smartphone or smartwatch to deliver clinical information to hospitals. Thus, the early detection of clinical cues can reduce the death rate of patients with acute disease. Nowadays, the daily habits of individuals in many developing countries have moved toward those of people in developed countries, thereby causing obesity and cardiovascular diseases. As such, the number of victims of these chronic diseases has gradually increased worldwide.

C-reactive protein (CRP) has been studied as an acute-phase protein biomarker for cardiovascular disease and

[a]*Department of Chemical Engineering, Kwangwoon University, 20 Kwangwoon-Ro, Nowon-Gu, Seoul 01897, Republic of Korea. E-mail: tlee@kw.ac.kr*
[b]*Department of Chemistry, Kwangwoon University, 20 Kwangwoon-Ro, Nowon-Gu, Seoul 01897, Republic of Korea*
[c]*School of Integrative Engineering, Chung-Ang University, Heukseok-dong, Dongjak-gu, Seoul 06910, Republic of Korea*

†Electronic supplementary information (ESI) available. See DOI: 10.1039/d0an02135k

inflammation.[16–18] CRP is synthesized in the liver and circulated within the plasma. Under healthy conditions for normal people, the concentration of CRP in plasma is usually less than 2.0 mg L^{-1}.[19] If the CRP concentration is increased to greater than 2.0 mg L^{-1}, this change can be considered to be because of the existence of cardiovascular disease, development of inflammation, and cancer formation. Thus, detection of CRP is one of the most important biomarkers within the *in vitro* diagnostics field.[20]

So far, various techniques have been developed to detect CRP concentrations precisely. The turbidimetric method, immunonephelometry, radio-immunodiffusion, and enzyme-linked immunosorbent assay (ELISA) have been widely used in hospital laboratories.[21,22] These conventional methods provide exact information on CRP determination; however, they require labor-intensive, time-consuming, and complicated detection steps that hamper testing efficiency. To solve this problem, several methods have been proposed to introduce nanotechnology for detecting CRP, including surface plasmon resonance,[23] fluorescence,[24] and Raman spectroscopy.[25]

As a robust alternative, the electrochemical detection of biomarkers provides several advantages, including rapid detection time, portability, a user-friendly interface, and an easy-to-handle apparatus.[26–28] Conventionally, antibodies have been used as the gold standard bioprobe for determining CRP concentrations. However, a recent CRP aptamer study demonstrated a similar binding affinity.[29,30] In addition, nucleic acid-based aptamers have various advantages compared to antibodies: (1) they can be synthesized by chemical production, which reduces manufacturing costs; (2) one can easily introduce functional groups to aptamers, such as amines and thiols, as well as fluorescence; and (3) the chemical production of aptamers is free of the ethical problems of antibodies produced by animals.[29] Several studies have reported aptamer-based CRP biosensors. However, certain studies still require a labeling process, requiring many sample volumes and a relatively higher LOD value.[31–33]

To overcome these problems, the present study developed an electrochemical biosensor composed of a multifunctional aptamer connected to a DNA four-way junction (4WJ) and a rhodium nanoplate heterolayer on a micro-gap electrode. The DNA 4WJ has four arms at the end of the fragment that can be used to introduce various functions at each arm (electron transfer mediation, immobilization, and target recognition). Within the head group of the DNA 4WJ, the CRP aptamer was tagged to target CRP binding. In the tail group of the DNA 4WJ, the thiol group was introduced for surface binding. The remaining two side arms had four Ag^+ ions for electron transfer mediation, which enhanced the electrochemical response. In addition, RhNPs were introduced for electron transfer facilitation.[34] To minimize CRP sample usage, the newly designed eight micro-gap electrode did not require an additional print-screen board, thereby lowering the costs of fabricating the biosensor. Fig. 1 shows the schematic diagram of the CRP biosensor in this study.

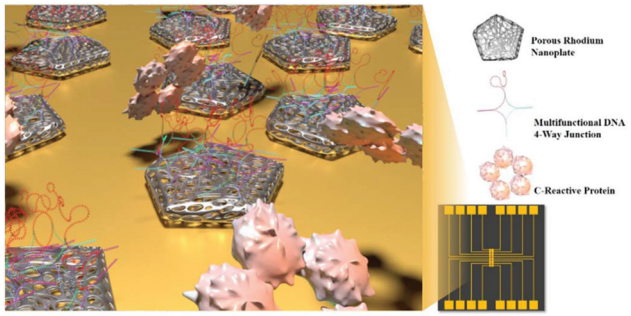

Fig. 1 Schematic illustration of the CRP biosensor; multifunctional DNA four-way junction/porous rhodium nanoplate heterolayer on the 2 × 8 array Au micro-gap electrode for binding CRP.

Experimental details

Materials

CRP was purchased from Sino Biological Inc. (China). CRP-Apt-4WJ-a (5′-CGA AGG GGA TTC GAG GGG TGA TTG CGT GCT CCA TTT GGT GTG CTG GAA CTC CCC GAC TGC-3′), SH-4WJ-b (5′-CCA GTC CCC CAG CCC ACA TAC TTT GTT GAT CC-Thiol-3′), 4WJ-c (5′-GGA TCA ATC ACC CCT GGC AA-3′), and 4WJ-d (5′-TTG CCA CCC CTG TGT ATG TGG GTT CCA GCA C-3′) were synthesized by Genotech (South Korea). All DNA stock solutions (100 μM) were stored with TE buffer solution (10 mM Tris-HCl, 1 mM EDTA).

All oligonucleotides were prepared in a TMS buffer containing 50 mM Tris, 100 mM NaCl, and 100 mM $MgCl_2$ before use. The working solution for CV and EIS contained 5 mM $K_3Fe(CN)_6$, 5 mM $K_4Fe(CN)_6$, 1 M KCl and 10 mM HEPES. For preparing the human serum, human male AB plasma (Sigma-Aldrich, USA) was used. Cysteamine, hemoglobin from horse hearts, interferon-γ from humans, immunoglobulin from goats, tumor necrosis factor-α from humans and troponin I from humans were purchased from Sigma-Aldrich (USA). Human serum was mixed with CRP samples diluted to different concentrations in PBS at the same rate. A mini-protein tetra cell and Power pacTM power supplies were purchased from Bio-Rad (USA) and used for gel electrophoresis. The results were confirmed with a UV transilluminator (Advance Co. Ltd., Japan). All experiments were performed in accordance with the Guidelines of Animal Experiment Guideline of Kwangwoon University and approved by the ethics committee at Kwangwoon University.

Fabrication of the micro-gap Au electrode

The design of the Au micro-gap electrode was carried out using AutoCAD (USA). The Au-micro-gap electrode was fabricated by the Korean Advanced Nano Fab Center (Daejon, Korea). The fabricated Au microgap had a size of 6.25 cm^2. The working area was 0.09 mm^2 and the gap between the two working areas was 10 μm. For cleaning the fabricated electrode, it was immersed in acetone solution with sonication for 10 min and then rinsed with ethanol and DI water succes-

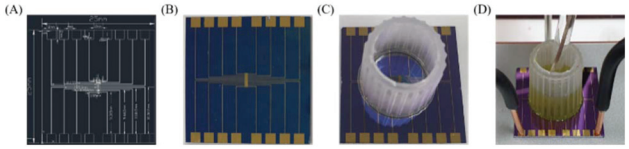

Fig. 2 (A) CAD image of the Au micro-gap electrode, (B) photo image of the Au micro-gap electrode, (C) photo image of the Au micro gap electrode with the working chamber (diameter 1.3 cm, height 1.5 cm) and (D) photo image of electrochemical measurement with the probe tip in the working solution.

sively. For the electrochemical measurements, a chamber was prepared with a diameter of 1.3 cm and a height of 1.5 cm and joined using polydimethylsiloxane (PDMS). In PDMS, Sylgard 184 a (USA) and Sylgard 184 b (USA) were mixed in a ratio of 10 : 1 and reacted in an oven at 70 °C for 1.5 h. Fig. 2 displays the fabrication process of the Au micro-gap electrode for the electrochemical CRP biosensor application.

Preparation of MF-4WJ/pRhNP on the Au micro-gap electrode

To immobilize the pRhNPs, 10 mM of cysteamine solution was dropped onto the prepared electrode for 1.5 h at room temperature, and then the pRhNPs were dropped onto the cysteamine-modified electrode for 1.5 h and allowed to self-assemble. To construct the multifunctional MF-DNA-4WJ, the MF-DNA-4WJ was dissolved in 10 μM of CRP-Apt-4WJ-a, SH-4WJ-b, 4WJ-c, and 4WJ-d composed of complementary sequences in tricaine mesylate (TMS) buffer with annealing at 80 °C for 5 min.

Then, it was cooled to 4 °C at a rate of 1 °C min^{-1}. Following the aforementioned procedure, 5 μM of the assembled MF-DNA-4WJ and 5 μM of $AgNO_3$ were treated and reacted at room temperature for 2 h. For each process, the substrate was washed with N_2 gas and distilled water.

Electrochemical analysis

All electrochemical experiments were conducted using AMETEK's Versastat3 (USA). The signals of cyclic voltammetry (CV) and electrochemical impedance spectroscopy (EIS) were detected in the working solution. CV was conducted within the potential range of −0.1–0.6 V at a scan rate of 0.1 V s^{-1}. EIS was conducted within the frequency range of 100 kHz–1 Hz with a signal amplitude of 10 mV. All electrochemical experiments were carried out using a conventional three-electrode system consisting of a Ag/AgCl reference electrode (CH Instruments, USA) and a micro-gap gold electrode as the working and auxiliary electrodes.

Results and discussion

Feasibility evaluation of the designed bioprobe

Referring to a previous study, it was determined that four consecutive C–C mismatched sequences were suitable, and a 4WJ bio-probe was designed so that eight Ag^+ ions were inserted into one bio-probe.[35] MF-DNA 4WJs consisted of four DNA sequences; CRP-Apt-4WJ-a is an aptamer sequence that selectively binds to CRP, SH-4WJ-b is a sequence modified with a thiol functional group for immobilization on a substrate, and 4WJ-c and 4WJ-d are sequences that are complementary to other sequences. 4WJ-a, b, c, and d are sequences complementary to each other, and there are four C–C mismatch sequences each. As Ag^+ ions can be inserted into the C–C mismatch sequence, an increase in the signal was expected.[36] The expected structure of MF-DNA 4WJs is described in Fig. 3(A).

Then, native TBM-PAGE (Tris-borate-magnesium chloride – polyacrylamide gel electrophoresis) was performed to confirm the assembly of MF-DNA-4WJs as designed (Fig. 3(B)). As a result, it was confirmed that the MF-DNA-4WJs were assembled through the annealing process; it was observed that the band that was not in lanes 2–5 was generated above lane 6. As a new band that was not in lane 6 was formed above lane 8, it can be seen that MF-DNA 4WJs and CRP bind well. However, seeing that no band was formed in lane 10, the MF-DNA 4WJs did not bind with bovine serum albumin (BSA). Thus, it was confirmed that MF-DNA-4WJs were formed and function as CRP-detecting bioprobes.

Electrochemical properties of the C–Ag–C structure

CV and EIS were performed to confirm whether an increase in the signal could be expected by inserting Ag^+ ions into the C–C mismatch sequence.

Fig. 4(A) shows the cyclic voltammograms of MF-4WJs and Ag ion-mismatched MF-4WJs. The redox current peak value (I_{pc}, I_{pa}) of the DNA-4WJs is 7.862 ± 0.419 μA at 333.31 ± 0.105 mV and −7.723 ± 0.409 μA at 216.23 ± 0.066 mV, and for DNA-4WJs with Ag^+ at 332.73 ± 0.916 mV, the redox current peak value (I_{pc}, I_{pa}) is 9.399 ± 0.478 μA and at 223.33 ± 0.921 mV it is −9.498 ± 0.551 μA. Ag^+ ions stabilize the C–C mismatched DNA to form a C–Ag–C structure, resulting in increased current intensity of I_{pc} and I_{pa} by 19% and 22%, respectively (Fig. 4(B)).

As a result of performing EIS under the same conditions, it was confirmed that charge transfer resistance (R_{ct}) decreased

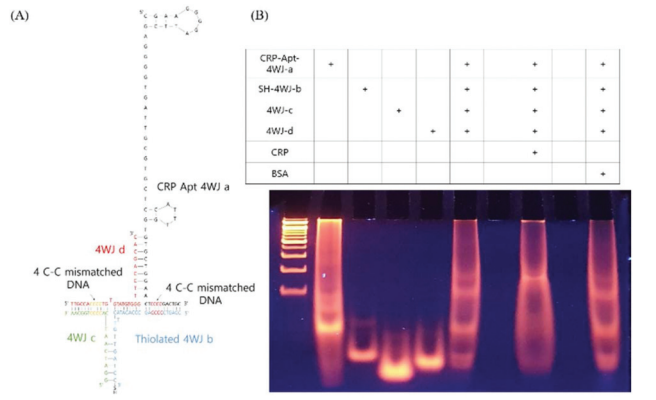

Fig. 3 (A) Folded schematic illustration of the MF-DNA 4WJ predicted by folding. (B) TBM-PAGE to confirm the feasibility of the MF-DNA-4WJ.

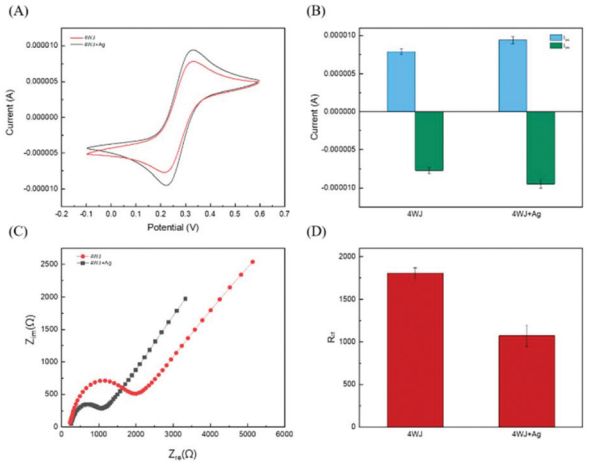

Fig. 4 (A) CV response at cysteamine/pRh/MF-DNA 4WJ (red line), cysteamine/pRh/MF-DNA 4WJ/Ag^+ (black line) in 5 mM $[Fe(CN)_6]^{3-/4-}$ and 10 mM HEPES buffer. (B) Redox peak current of cysteamine/pRhNP/MF-DNA 4WJ and cysteamine/pRhNP/MF-DNA 4WJ/Ag^+. (C) Nyquist plot of electrochemical impedance spectra in 5 mM $[Fe(CN)_6]^{3-/4-}$ and 10 mM HEPES buffer, cysteamine/pRh/MF-DNA-4WJs (red dotted line), and cysteamine/pRh/MF-DNA 4WJ/Ag^+ (black dotted line). (D) R_{ct} of cysteamine/pRh/MF-DNA 4WJ and cysteamine/pRh/MF-DNA 4WJ/Ag^+.

by 40% when Ag^+ ions were inserted into the MF-DNA-4WJs (Fig. 4(C)). Based on the results, Ag^+ strongly promotes electron movement, thereby enhancing the electrochemical signal. As the signal change width of R_{ct} is greater than the peak current, the change in R_{ct} was determined as a detection method (Fig. 4(D)).

Electrochemical analysis of the CRP/MF-DNA 4WJ on pRhNP modified electrodes

After thoroughly cleaning the prepared Au micro-gap electrode with N_2 gas and distilled water, the MF-DNA-4WJ/pRhNP was prepared by a self-assembly process. Each process was confirmed by CV and EIS in 10 mM HEPES, 1 M KCl, and 5 mM $K_{3/4}Fe(CN)_6$. In the presence of $[Fe(CN)_6]^{3-/4-}$, in the electrolyte solution, electrons were exchanged with the exposed portion of the electrode surface. The exchange of electrons between $[Fe(CN)_6]^{3-/4-}$ and the electrode surface caused the following redox reaction:

$$[Fe(CN)_6]^{3-} + e^- \leftrightarrow [Fe(CN)_6]^{4-}$$

As the generated redox current is proportional to the area of the electrode surface, it was expected that the redox current of the electrode modified using the pRhNPs would increase. The I_{pc} and I_{pa} of the pRh-modified electrode were 12.703 ± 0.857 μA at 325.45 ± 0.617 mV and −12.294 ± 0.801 μA at 223.74 ± 0.534 mV, respectively.

The I_{pc} and I_{pa} of the bare electrode were 8.462 ± 0.527 μA at 332.91 ± 0.717 mV and −8.225 ± 0.579 μA at 208.82 ± 0.734 mV, respectively. Comparing the two results, it was confirmed that the redox current increased in the electrode modified with pRh compared to the bare electrode. The binding of MF-DNA-4WJs and CRP on the modified electrode surface blocks the redox current so that I_{pc} was decreased from 332.73 ± 0.916 mV, 9.399 ± 0.478 μA to 329.48 ± 0.756 mV, 7.88 ± 0.628 μA, while I_{pa} was decreased from 223.33 ± 0.921 mV, −9.498 ± 0.551 μA to 198.29 ± 0.731 mV, −7.57 ± 0.643 μA. Fig. 5(A) depicts the cyclic voltammogram and Fig. 5(B) depicts the redox peak current values of the fabricated CRP/MF-DNA-4WJ on the pRhNP-modified electrode.

Fig. 5(C) shows the EIS results for the bare electrode on a complex plane (Nyquist plot), and the resistance of the working solution (R_s) and surface R_{ct} were calculated using the intersection of the semicircle and the horizontal axis of the Nyquist plot.

In the low-frequency region, the electrochemical reaction is under mass transfer diffusion control because the change in the concentration at the electrode surface owing to current change is slow. This effect was expressed as Warburg impedance (Z_w).[37]

The sensing system configuration proposed in this study can be modeled as an ideal Randles circuit consisting of R_{ct} connected in series with R_s, Warburg impedance, and electric double layer capacitance (C_{dl}) at the electrode surface connected in parallel. As a result of plotting the EIS results from the bare electrode, it was confirmed that the behavior was similar to the actual experimental result. R_{ct} can be easily obtained from the intersection of the horizontal axis and the semicircle of the Nyquist plot. Therefore, R_{ct} was measured for each fabrication step (Fig. 5(D)). As a result, it was confirmed that the R_{ct} value decreased from 1528.886 ± 136.8719 Ω to 613.2214 ± 44.10302 Ω when the bare electrode was modified with pRh, and when DNA-4WJs were combined with CRP, the

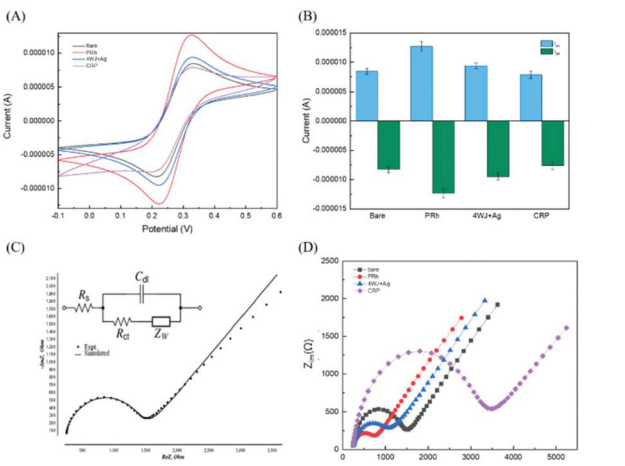

Fig. 5 (A) Cyclic voltammogram and (B) redox peak current values of the fabricated CRP/MF-DNA-4WJ on the pRhNP-modified electrode. (C) Nyquist plot of a comparison between experimental data and simulation using the Randles circuit. (D) EIS during fabrication process in working solution; bare electrode (black line), cysteamine/pRhNP (red line), cysteamine pRhNP/MFDNA-4WJs/Ag^+ (blue line), and cysteamine/pRhNP/MF-DNA-4WJs/Ag^+/CRP (purple line).

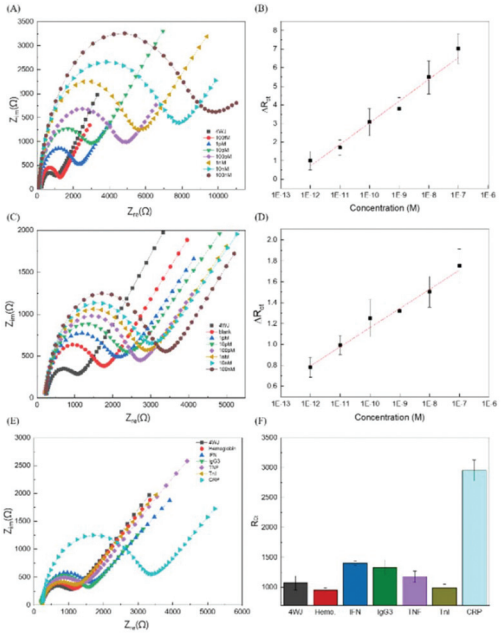

Fig. 6 (A) Electrochemical impedance spectra at different concentrations of CRP diluted with PBS buffer in 10 mM HEPES and 5 mM $[Fe(CN)_6]^{3-/4-}$. (B) Linear regression curve of different CRP concentrations; linear range from 100 nM to 1 pM. (C) Electrochemical impedance spectra at different concentrations of CRP diluted with 20% human serum in 10 mM HEPES and 5 mM $[Fe(CN)_6]^{3-/4-}$. (D) Linear regression curve of different CRP concentrations in 20% human serum; linear range from 100 nM to 1 pM. (E) Electrochemical impedance spectra for several proteins present in human serum. (F) R_{ct} of several proteins present in human serum.

R_{ct} value increased significantly from 1069.296 ± 158.218 Ω to 2230.9 ± 487.358 Ω. Through this, it was shown that pRhNPs offered a more active region and higher coverage. Moreover, the surface investigations of the pRhNP-modified electrode, pRhNP/MF-DNA-4WJ-modified electrode and CRP on the MF-DNA-4WJ on the pRhNP electrode were carried out by atomic force microscopy successively (Fig. S1†).[38,39]

Biosensor performance

To evaluate the sensitivity and detection limit of the fabricated biosensor, EIS was performed in the CRP concentration range of 1 pM to 100 nM and the results are shown in Fig. 6(A). It is plotted as a Nyquist plot. The EIS results were used to monitor electron transfer when the bioprobe and CRP target protein were bound through R_{ct} measured at the working electrode. As expected, the $R_s + R_{ct}$ value increased to ~3 kΩ when combined with 1 pM CRP, whereas for the electrode modified with pRh/DNA-4WJs, it was ~2 kΩ. As the CRP concentration was increased, it was confirmed that the $R_s + R_{ct}$ value increased to ~12 kΩ. The change in R_{ct} based on the binding of the CRP target protein to the bioprobe was expressed as a percentage as follows.

$$\Delta R_{ct} = \frac{R_{ct,bioprobe\text{-}CRP} - R_{ct,bioprobe}}{R_{ct,bioprobe}},$$

where $R_{ct,bioprobe}$ is the charge transfer resistance of the manufactured sensor and $R_{ct,bioprobe\text{-}CRP}$ is the charge transfer resistance when the sensor and the CRP target protein of each concentration react. Using ΔR_{ct}, a linear regression curve with an intercept of 14.68878 ± 0.92674 and a slope of 1.16486 ± 0.08961 (R^2 = 0.97688) is shown in Fig. 6(B). Thus, the limit of detection (LOD) of this sensor was 0.349 pM (at S/N = 3).

In order to confirm whether the manufactured sensor can be used in actual clinical practice, CRP diluted in 20% human serum was prepared and EIS was performed within a concentration range of 1 pM–100 nM (Fig. 6(C)).

The $R_s + R_{ct}$ value increased to ~5 kΩ when combined with CRP, whereas for the electrode modified with pRh/DNA-4WJs, it was ~2 kΩ. Similarly, using ΔR_{ct}, a linear regression curve with a slope of 0.1833 ± 0.00988 and an intercept of 2.99421 ± 0.9953 was obtained (R^2 = 0.98852), as shown in Fig. 6(D). The LOD calculated using this regression curve was 3.55 fM (at S/N = 3).

In addition, in order to confirm the selectivity of the manufactured sensor, EIS was performed after reacting with different proteins (hemoglobin: red, interferon-γ: blue, immunoglobulin 3: green, tumor necrosis factor-α: purple, and troponin I: grass green) of the same concentration in a 20% human serum sample (Fig. 6(E)). As a result of performing the selectivity test, the R_{ct} value of proteins other than CRP was ~1.3 kΩ, whereas the CRP target protein showed a high R_{ct} of 3 kΩ (Fig. 6(F)). Therefore, the high selectivity of the manufactured sensor was confirmed. Table 1 shows the comparison table of electrochemical CRP biosensors.

Table 1 Comparison of this study with other studies for CRP detection

Probe	Detection method	LOD	Linear range	Label free	Ref.
Antibody	EIS	176 ± 18 pM	0.5–50 nM	O	20
RNA aptamer/antibody	SWV	0.0017 ng mL^{-1}	0.005–125 ng mL^{-1}	X	31
DNA aptamer	SWV	1 pM	1–100 pM	O	32
RNA aptamer/antibody	DPV	0.54 μg L^{-1}	0.1–50 mg L^{-1}	X	33
Antibody/antibody	DPV	0.33 fg mL^{-1}	1–100 ng mL^{-1}	X	40
Antibody/antibody	ASV	0.05 ng mL^{-1}	0.2–100 ng mL^{-1}	X	41
Antibody	EIS	—	3.125–25 mg L^{-1}	O	42
Antibody/antibody	EIS	1.5 ng mL^{-1}	0.01–150 μg mL^{-1}	X	43
DNA aptamer	EIS	0.349 pM (0.08 ng L^{-1})	1 pM–100 nM (0.23 ng L^{-1}–2.3 mg L^{-1})	O	This work

Conclusions

The present study proposed an electrochemical biosensor composed of Ag-inserted MF-DNA 4WJs and pRhNPs on a Au micro-gap electrode for CRP detection. The durability of the biosensor was improved by the introduction of pRhNPs that maintained the redox property for 10 days (Fig. S2†). In addition, eight Ag^+ ions were inserted into the C–C mismatch of DNA-4WJs to increase the conductivity, thereby improving the sensitivity of the sensor. Also, the Au-micro-gap electrode provides eight-time repeatability, which confirmed the reliability of CRP determination. An experiment to confirm the sensitivity and selectivity of the biosensor was conducted using human serum and a calibration curve was obtained. Plasma CRP levels may rise as much as 1000 fold or more after acute inflammation stimulation, and under normal healthy conditions for people plasma CRP levels are less than 2 mg L^{-1}. The sensor proposed in this study has a wide linear range of 0.23 ng L^{-1} to 2.3 mg L^{-1}. Therefore, through this study, it is possible to detect from a normal range to a high level of CRP through stimulation such as inflammation, AMI, *etc*. So this sensor is expected to be of great clinical value.

Conflicts of interest

There are no conflicts to declare.

Acknowledgements

This research was supported by the Basic Science Research Program through the National Research Foundation of Korea (NRF) funded by the Ministry of Education (2018R1D1A1B07049407) and by Korea Environmental Industry and Technology Institute (KEITI) through the program for the management of aquatic ecosystem health, funded by the Korean Ministry of Environment (MOE). (2020003030001) and by the Industrial Core Technology Development Program (20009121, Development of early diagnostic system of peritoneal fibrosis by multiplex detection of exosomal nucleic acids and protein markers) and funded by the Ministry of Trade, Industry and Energy (MOTIE, Korea).

References

1 T. M. Allen and P. R. Cullis, *Adv. Drug Delivery Rev.*, 2013, **65**, 36–48.
2 V. P. Torchilin, *Annu. Rev. Biomed. Eng.*, 2006, **8**, 343–375.
3 L. E. Cahill, M. L. Bertoia, S. A. Aroner, K. J. Mukamal and M. K. Jensen, *Curr. Diabetes Rep.*, 2015, **15**, 88.
4 T. A. Pearson, G. A. Mensah, R. W. Alexander, J. L. Anderson, R. O. Cannon, M. Criqui, Y. Y. Fadl, S. P. Fortmann, Y. Hong, G. L. Myers, N. Rifai, S. C. Smith, K. Taubert, R. P. Tracy and F. Vinicor, *Circulation*, 2003, **107**, 499–511.
5 H. Radecka and J. Radecki, *J. Mex. Chem. Soc.*, 2015, **59**, 269–275.
6 X. Huang, D. Xu, J. Chen, J. Liu, Y. Li, J. Song, X. Ma and J. Guo, *Analyst*, 2018, **143**, 5339–5351.
7 Z. Altintas, W. M. Fakanya and I. E. Tothill, *Talanta*, 2014, **128**, 177–186.
8 S. Mythili and N. Malathi, *Biomed. Rep.*, 2015, **3**, 743–748.
9 F. L. Ng, M. Saxena, F. Mahfoud, A. Pathak and M. D. Lobo, *Curr. Hypertens. Rep.*, 2016, **18**, 61.
10 S. H. Park, Y. Zhang, J. A. Rogers and L. Gallon, *Curr. Opin. Nephrol. Hypertens.*, 2019, **28**, 390–396.
11 W. Y. Lai, J. W. Wang, B. T. Huang, E. P. Y. Lin and P. C. Yang, *Theranostics*, 2019, **9**, 1741–1751.
12 A. Florea, G. Melinte, I. Simon and C. Cristea, *Biosensors*, 2019, **9**, 1–15.
13 Y. Lu, Z. Shi and Q. Liu, *Curr. Opin. Food Sci.*, 2019, **28**, 74–81.
14 T. Lee, M. Mohammadniaei, H. Zhang, J. Yoon, H. K. Choi, S. Guo, P. Guo and J.-W. Choi, *Adv. Sci.*, 2020, **7**, 1902477.
15 S. Patel, R. Nanda, S. Sahoo and E. Mohapatra, *Biochem. Res. Int.*, 2016, **2016**, 3130469.
16 L. Guo, S. Liu, S. Zhang, Q. Chen, M. Zhang, P. Quan, J. Lu and X. Sun, *Sci. Rep.*, 2015, **5**, 1–8.
17 A. M. Dupuy, S. Badiou, B. Descomps and J. P. Cristol, *Clin. Chem. Lab. Med.*, 2003, **41**, 948–949.
18 N. R. Sproston and J. J. Ashworth, *Front. Immunol.*, 2018, **9**, 1–11.
19 M. Thangamuthu, C. Santschi and O. J. F. Martin, *Biosensors*, 2018, **8**, 34.
20 T. Bryan, X. Luo, P. R. Bueno and J. J. Davis, *Biosens. Bioelectron.*, 2013, **39**, 94–98.
21 H. Riese, T. G. M. Vrijkotte, P. Meijer, C. Kluft and E. J. C. de Geus, *BMC Cardiovasc. Disord.*, 2002, **2**, 1–12.
22 R. Ramamoorthy, V. Nallasamy, R. Reddy, N. Esther and Y. Maruthappan, *J. Pharm. BioAllied Sci.*, 2012, **4**, 422.
23 W. Wang, Z. Mai, Y. Chen, J. Wang, L. Li, Q. Su, X. Li and X. Hong, *Sci. Rep.*, 2017, **7**, 1–8.
24 K. M. Park, D. J. Chung, M. Choi, T. Kang and J. Jeong, *Nano Convergence*, 2019, **6**, 35.
25 M. S. Bergholt and S. Hassing, *Analyst*, 2009, **134**, 2123–2127.
26 S. Y. Park, J. Kim, G. Yim, H. Jang, Y. Lee, S. M. Kim, C. Park, M. H. Lee and T. Lee, *Colloids Surf., B*, 2020, **195**, 111240.
27 T. Lee, J. H. Ahn, J. Choi, Y. Lee, J. M. Kim, C. Park, H. Jang, T. H. Kim and M. H. Lee, *Micromachines*, 2019, **10**, 203.
28 S. N. Topkaya, M. Azimzadeh and M. Ozsoz, *Electroanalysis*, 2016, **28**, 1402–1419.
29 S. Wildner, S. Huber, C. Regl, C. G. Huber, U. Lohrig and G. Gadermaier, *Sci. Rep.*, 2019, **9**, 1–14.
30 Y. Zhang, B. S. Lai and M. Juhas, *Molecules*, 2019, **24**, 941.
31 J. Wang, J. Guo, J. Zhang, W. Zhang and Y. Zhang, *Biosens. Bioelectron.*, 2017, **95**, 100–105.
32 M. Jarczewska, J. Rębiś, Ł. Górski and E. Malinowska, *Talanta*, 2018, **189**, 45–54.

33 S. Centi, L. B. Sanmartin, S. Tombelli, I. Palchetti and M. Mascini, *Electroanalysis*, 2009, **21**, 1309–1315.
34 S. Kang, W. Shin, M. Choi, M. Ahn, Y. Kim, S. Kim, D. Min and H. Jang, *ACS Nano*, 2018, **12**, 6997–7008.
35 M. Mohammadniaei, J. Yoon, T. Lee, B. G. Bharate, J. Jo, D. Lee and J. Choi, *Small*, 2018, **14**, 1703970.
36 H. Torigoe, I. Okamoto, T. Dairaku, Y. Tanaka, A. Ono and T. Kozasa, *Biochimie*, 2012, **94**, 2431–2440.
37 S. R. Taylor and E. Gileadi, *Corrosion*, 1995, **51**, 664–671.
38 T. Lee, S.-U. Kim, J. Min and J.-W. Choi, *Adv. Mater.*, 2010, **22**, 510–514.
39 T. Lee, A. Y. Kumar, F. Pi, A. Sharma and J.-W. Choi, *ACS Nano*, 2015, **9**, 6675–6682.
40 J. Zhang, W. Zhang, J. Guo, J. Wang and Y. Zhang, *Anal. Biochem.*, 2017, **539**, 1–7.
41 C. Kokkinos, M. Prodromidis, A. Economou, P. Petrou and S. Kakabakos, *Anal. Chim. Acta*, 2015, **886**, 29–36.
42 T. Songjaroen, R. M. Feeny, M. M. Mensack, W. Laiwattanapaisal and C. S. Henry, *Sens.Biosensing Res.*, 2016, **8**, 14–19.
43 S. Jampasa, W. Siangproh, R. Laocharoensuk, T. Vilaivan and O. Chailapakul, *Talanta*, 2018, **183**, 311–319.